

“Surface chemical and thermodynamic controls on bacterial metal reduction in subsurface environments”

E.E. Roden¹

¹*The University of Alabama, Tuscaloosa, AL, eroden@bsc.as.ua.edu.*

1 INTRODUCTION

Understanding the geochemical controls on microbial reduction of soluble and solid-phase metals is a prerequisite for development of reactive transport models of inorganic contaminants and radionuclides in subsurface environments. Fe(III) oxides are ubiquitous components of soils and sediments, and often provide the largest source of electron-accepting capacity for bacterial metal reduction in subsurface environments (Lovley, 1991). Fe(III) oxides occur in a variety of phases in natural environments, ranging from poorly crystalline ferrihydrite to well-crystallized minerals such as goethite and hematite (Cornell and Schwertmann, 1996). The studies described herein were designed to explore how the surface chemical (e.g. specific surface area) and thermodynamic properties (e.g. oxide reduction potential) of Fe(III) oxides influence the rate and extent of bacterial Fe(III) oxide reduction. The results permit development of conceptual and quantitative models of enzymatic Fe(III) oxide reduction at circumneutral pH that can be compared and contrasted with models of abiotic mineral dissolution and soluble metal reduction.

2 MATERIALS AND METHODS

2.1 *Fe(III) oxide phases*

The Fe(III) oxides employed in this study included a variety of pure synthetic phases (Roden, 2003) as well as three previously characterized Fe(III) oxide-bearing subsoil or subsurface materials (HC, CP, and Oyster). The HC and CP materials are Fe(III) oxide/layered silicate mixtures obtained from Ultisols in Tennessee and North Carolina, respectively. The Oyster material is Fe(III) oxide-coated sand from Pleistocene Age Atlantic Coastal Plain sediments. More detailed descriptions of the properties of these materials are available elsewhere (Zachara et al., 1989; Zachara et al., 1995; Roden, 2004). The synthetic Fe(III) oxides were freeze-dried and passed through a 100- μm sieve, and their specific surface area determined by multipoint BET N_2 adsorption. The natural materials were air dried and passed through a 2 mm sieve prior to use in experiments.

2.2 *Bacterial reduction experiments*

The synthetic and natural Fe(III) oxide-bearing solids were suspended in sterile, anaerobic Pipes buffer (10 mM, pH 6.8) contained in sealed serum vials to obtain a Fe(III) concentration of ca. 10 mmol L^{-1} . Other experiments were conducted with soluble Fe(III) citrate (50 mM) or U(VI)-carbonate (0.01-1 mM) as electron acceptors. The electron donor for metal reduction was either 100% H_2 in the vial headspace, or 10 mM of either sodium lactate or sodium acetate. The medium was inoculated with ca. 10^8 cells mL^{-1} of either tryptic soy broth-grown *Shewanella putrefaciens* strain CN32 cells, or acetate/fumarate-grown *Geobacter sulfurreducens* cells. Samples for determination of dissolved (0.2- μm filtration and

Ferrozine analysis) and total Fe(II) (0.5M HCl extraction and Ferrozine analysis) and pH were collected at 1-10 d intervals.

2.3 Ascorbate and AH₂DS reduction experiments

The synthetic and natural Fe(III) oxide-bearing solids were suspended in anaerobic 10 mM ascorbic acid or 10 mM AH₂DS (the reduced form of AQDS, anthroquinone-2,6-disulfonate, prepared by reacting AQDS with 100% H₂ gas in the presence of a palladium catalyst). The oxide suspensions were incubated at room temperature on a rotary shaker (250 rpm) and samples were removed with a N₂-flushed plastic syringe at regular intervals. A portion of the sample was passed through a 0.2- μ m filter into Ferrozine for Fe(II) analysis, and the remainder used for determination of pH. The final (after reduction ceased) dissolved Fe(II) concentration and pH values achieved in the AH₂DS reduction experiments were used in conjunction with the E_h^0 of the AQDS/AH₂DS couple (+0.23V; Clark, 1960) to estimate the reduction potential (E_h^0) of the synthetic and natural Fe(III) oxide phases.

3 RESULTS AND DISCUSSION

3.1 Initial rates of reduction

Initial surface area-specific rates of bacterial reduction of the synthetic Fe(III) oxides were independent of oxide surface area and E_h^0 (Fig. 1A). In contrast, rates of abiotic Fe(III) oxide reduction by ascorbate and AH₂DS were significantly correlated with oxide surface area and E_h^0 (Fig. 1B).

3.2 Long-term extent of reduction

Similar patterns of Fe(II) accumulation were observed during long-term (3-week incubation) reduction of the various synthetic Fe(III) oxides by *G. sulfurreducens* (Fig. 2A). Measurements of dissolved Fe(II) and pH during the reduction experiments, together with the estimated E_h^0 values for the different Fe(III) oxides, were used to compute the free energy of Fe(III) oxide reduction for the different synthetic phases during the course of the reduction experiments. The results (Fig. 3) indicate that the cessation of oxide reduction activity could not be attributed to free energy constraints posed by dissolved Fe(II) accu-

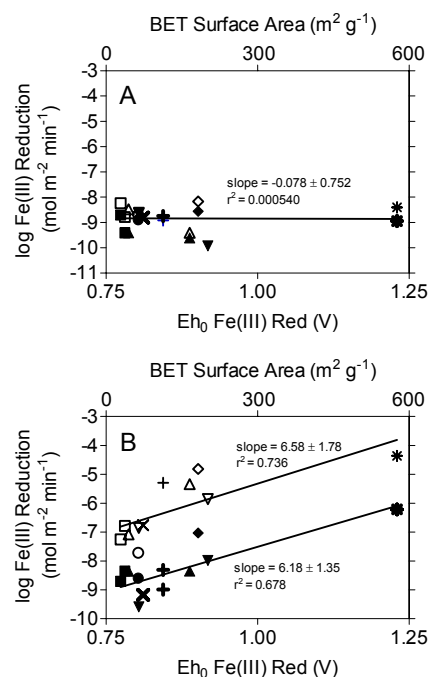


Figure 1. Initial (2-3 day incubation) surface area-specific rates of bacterial (A) and abiotic (B) reduction of synthetic Fe(III) oxides. Different symbols correspond to different Fe(III) oxide phases. Open and closed symbols in panel A refer to data for *S. putrefaciens* and *G. sulfurreducens*, respectively. Open and closed symbols in panel B refer to data for AH₂DS and ascorbic acid reduction, respectively.

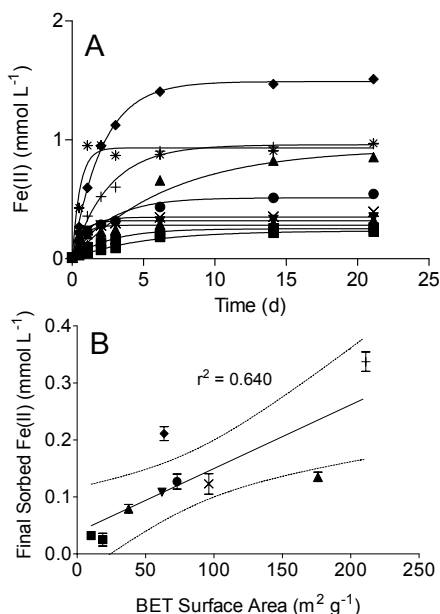


Figure 2. Total (0.5M HCl extraction) Fe(II) production (A) and final sorbed Fe(II) (total minus dissolved Fe(II)) concentration during reduction of synthetic Fe(III) oxides by *G. sulfurreducens*. Different symbols correspond to different Fe(III) oxide phases. Lines in panel A show nonlinear regression fits of the data to the an equation depicting the accumulation of end-product of a first-order reaction. Line in panel shows result of a linear least-squares regression analysis.

the bacterial reduction experiments (Fig. 4B, solid symbols). However, when the analysis was restricted to the long-term “microbially-reducible” fraction of the Fe(III) oxide content of the natural solids (Fig. 4B, open symbols), the data could be well-approximated with γ values of ca. 1, i.e. by a first-order rates process. Kinetic and thermodynamic considerations indicated that neither the abundance of electron donor (lactate) nor the accumulation of aqueous end-products of oxide reduction (Fe(II), acetate, dissolved inorganic carbon) are likely to have posed significant limitations on the long-term kinetics of oxide reduction. Rather, accumulation of biogenic Fe(II) on residual oxide surfaces appeared to play a dominant role in governing the long-term kinetics of bacterial crystalline Fe(III) oxide reduction. This assertion is supported by the correlation between oxide surface area the quantity of sorbed Fe(II) present at the end of the synthetic Fe(III) oxide reduction experiments (Fig. 2B).

mulation and pH increase, because reduction rates approached zero at ΔG_{rxn} values substantially lower than the theoretical minimum of ca. -20 kJ mol^{-1} required for energy conservation during biological energy metabolism (Schink, 1997).

3.3 Reduction of natural Fe(III) oxide phases

Data from long-term experiments on bacterial and abiotic reduction of natural Fe(III) oxides (Fig. 4) were interpreted in relation to a standard a generalized rate law for mineral dissolution

$$J_t/m_0 = k'(m/m_0)^\gamma \quad (1)$$

where J_t is the rate of dissolution and/or reduction at time t , m_0 is the initial mass of oxide, and m/m_0 is the unreduced or undissolved mineral fraction) in order to evaluate changes in the apparent reactivity of Fe(III) oxides during long-term biological vs. chemical reduction. The natural Fe(III) oxide assemblages demonstrated significant changes in reactivity during long-term abiotic reductive dissolution (Fig. 4A), as indicated by γ values in excess of 1 for curve-fits of the data to the generalized rate law. Much larger changes in reactivity were estimated for

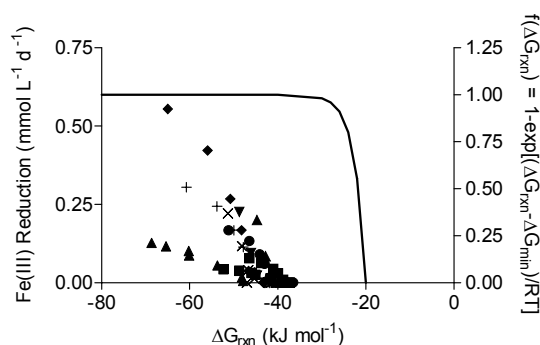


Figure 3. Rate of Fe(III) reduction during long-term *G. sulfurreducens* experiments as a function of the estimated free energy of reaction (ΔG_{rxn}). Fe(III) reduction rates were computed from the nonlinear curve-fits shown in Fig. 2. The solid line shows the relationship between reaction rate and energetics predicted based on transition state theory Lasaga (1998).

3.4 General discussion and conclusions

The experimental findings support a conceptual model of bacterial Fe(III) oxide reduction kinetics that differs fundamentally from established models of abiotic Fe(III) oxide reductive dissolution in that oxide surface area exerts primary control on both the initial rate *and* the long-term extent of reduction. Numerical simulations of surface area-controlled biotic vs. abiotic Fe(III) oxide reduction indicate that this conceptual model can account for the pseudo-first order kinetics of reduction of the operationally-defined “microbially-reducible” fraction of the sediment Fe(III) oxide pool (Roden, 2004). The explicit surface area control of the initial rate and extent of oxide reduction leads to rate formulations for oxide reduction as a function of (i) electron acceptor abundance, and (ii) the density of dissimilatory metal-reducing bacteria (DMRB), that differ from those for reduction of soluble metals such as chelated Fe(III) and U(VI)-carbonate species. Rates of solid-phase Fe(III) oxide reduction are a linear function of reactive surface site density and a hyperbolic (Monod-style) function of DMRB. The latter relationship is analogous to the well-recognized hyperbolic dependence of abiotic reductive dissolution rate on ligand concentration (Hering and Stumm, 1990). In contrast, rates of soluble metal reduction are a hyperbolic function of metal concentration and a linear function of DMRB abundance.

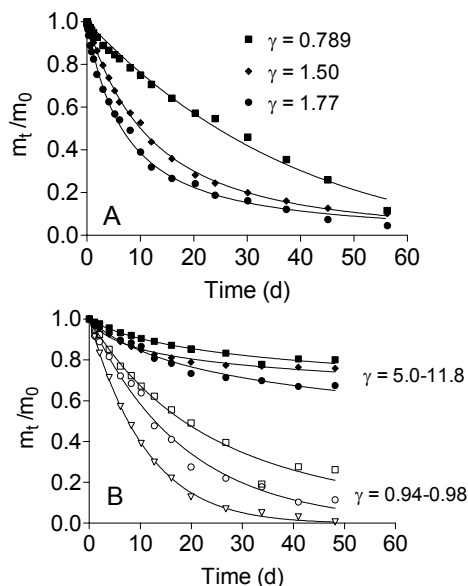


Figure 4. Kinetics of ascorbate (A) and bacterial (B) reduction of natural Fe(III) oxide-bearing materials. Squares, diamonds, and triangles represent the HC, CP, and Oyster materials, respectively. Open symbols in panel B refer to reduction of the “microbially-available” fraction of the oxide pool. The terms m_0 and m_t refer to the mass (concentration) of Fe(III) oxide present at the start of the experiment and at time t , respectively. Solid lines show nonlinear regression fits of the data to the integrated form of the generalized mineral dissolution rate law (Eqn. 1 in text). γ values refer to the results of the nonlinear curve fits.

3.5 References

- Clark, W. M. 1960. Oxidation-Reduction Potentials of Organic Systems. The Williams and Wilkins Company, Baltimore.
- Cornell, R. M., and U. Schwertmann. 1996. The Iron Oxides. VCH, New York.
- Hering, J. G., and W. Stumm. 1990. Oxidative and reductive dissolution of minerals. In M. F. Hochella, and A. F. White (eds.). Mineral-water interface geochemistry, pp. 427-464. Mineralogical Society of America, Washington, DC.
- Lasaga, A. C. 1998. Kinetic theory in the earth sciences. Princeton University Press, Princeton.
- Lovley, D. R. 1991. Dissimilatory Fe(III) and Mn(IV) reduction. Microbiol. Rev. 55:259-287.
- Roden, E. E. 2003. Fe(III) oxide reactivity toward biological versus chemical reduction. Environ. Sci. Technol. 37:1319-1324.
- Roden, E. E. 2004. Analysis of long-term bacterial versus chemical Fe(III) oxide reduction kinetics. Geochim. Cosmochim. Acta Submitted for publication.
- Schink, B. 1997. Energetics of syntrophic cooperation in methanogenic degradation. Microbiol. Mol. Biol. Rev. 61:262-280.
- Zachara, J. M., S. C. Smith, and L. S. Kuzel. 1995. Adsorption and dissociation of Co-EDTA complexes in Fe oxide containing subsurface soils. Geochim. Cosmochim. Acta 59:4825-4844.
- Zachara, J. M., C. C. Ainsworth, C. E. Cowan, and C. T. Resch. 1989. Adsorption of chromate by subsurface soil horizons. Soil Sci. Soc. Am. J. 53:418-428.